



Special Topic Cluster

Templated Reactive Crystallization of Active Pharmaceutical Ingredient in Hydrogel Microparticles Enabling Robust Drug Product Processing



Purnima N. Manghnani^a, Luke Schenck^e, Saif A. Khan^{d,a,*}, Patrick S. Doyle^{a,b,c,*}

^a Singapore-MIT Alliance for Research and Technology, 1 CREATE Way, #04-13/14 Enterprise Wing 138602, Singapore

^b Department of Chemical Engineering, Massachusetts Institute of Technology, 77 Massachusetts Avenue Room E17-504F, Cambridge, MA, 02139 USA

^c Harvard Medical School Initiative for RNA Medicine, Boston, MA, 02115 USA

^d Department of Chemical and Biomolecular Engineering, National University of Singapore, 4 Engineering Drive 4, Singapore 117585, Singapore

^e Process Research and Development, Merck & Co., Inc., 126 E. Lincoln Ave Rahway NJ 07065, USA

ARTICLE INFO

Article history:

Received 21 February 2023

Revised 4 May 2023

Accepted 4 May 2023

Available online 7 May 2023

Keywords:

Pharmaceutical

Salt form

Hydrogels

Reactive crystallization

ABSTRACT

Commercialization of most promising active pharmaceutical ingredients (APIs) is impeded either by poor bioavailability or challenging physical properties leading to costly manufacture. Bioavailability of ionizable hydrophobic APIs can be enhanced by its conversion to salt form. While salt form of the API presents higher solution concentration than the non-ionized form, poor physical properties resulting from particle anisotropy or non-ideal morphology (needles) and particle size distribution not meeting dissolution rate targets can still inhibit its commercial translation. In this regard, API physical properties can be improved through addition of non-active components (excipients or carriers) during API manufacture. In this work, a facile method to perform reactive crystallization of an API salt in presence of the microporous environment of a hydrogel microparticle is presented. Specifically, the reaction between acidic antiretroviral API, raltegravir and base potassium hydroxide is performed in the presence of polyethylene glycol diacrylamide hydrogel microparticles. In this bottom-up approach, the spherical template hydrogel microparticles for the reaction lead to monodisperse composites loaded with inherently micronized raltegravir-potassium crystals, thus improving API physical properties without hampering bioavailability. Overall, this technique provides a novel approach to reactive crystallization while maintaining the API polymorph and crystallinity.

© 2023 American Pharmacists Association. Published by Elsevier Inc. All rights reserved.

Introduction

The success of a drug formulation depends on its ability to transport the API to its target site at a therapeutically relevant concentration. This is particularly challenging for the oral drug delivery route as the API is subjected to various biological barriers in the gastrointestinal tract followed by first pass metabolism. Moreover, 90% of drugs in the development pipeline have hydrophobic APIs which results in restricted bioavailability.^{1,2} To improve bioavailability, salt formation of ionizable hydrophobic APIs offers a facile approach. It serves as a strategy to improve aqueous solubility, stability and alter gastrointestinal absorption.^{3,4} For instance, oral formulations of diclofenac contain its potassium or sodium salts which possess different dissolution profiles thereby exhibiting different pharmacokinetic behavior.⁵ Currently, about 50% of APIs are administered as salts,

indicating the importance of salt formulations.⁶ Typically, APIs possessing acidic or basic functional groups are amenable to salt formation. Reactive crystallization, a widely used approach to precipitate salt APIs occurs when synthesis of the API salt drives supersaturation.⁷ As the neutralization reaction between the ionized parent API and a suitable counterion leads to salt formation in solution, its concentration at a certain point exceeds solubility leading to crystalline product formation. Processes involving reactive crystallization can be used for synthesizing a product or for its purification from a multi-component system.

Apart from bioavailability, physical properties of API crystals such as particle size, size distribution, morphology, surface roughness and hardness govern its commercial translation. Undesirable API properties can result in a number of processing difficulties such as uneven powder feeding, inconsistent blend formation, poor compression and sticking to process equipment.⁸ While conventional particle engineering like milling of bulk crystals,⁹ co-crystal formation or sophisticated crystallization techniques to obtain specific crystal morphology have

* Corresponding authors.

E-mail addresses: saifkhan@nus.edu.sg (S.A. Khan), pdoyle@mit.edu (P.S. Doyle).

shown success, several APIs with challenging morphologies like needles cannot be processed via these routes.¹⁰ Another potential method to optimize API physical properties is to incorporate a non-active component during particle formation leading to a co-processed form.¹¹ For instance, developing co-processed API particles through techniques like co-precipitation through spray drying^{12,13} or solvent exchange in micro-droplets,^{14,15} micro or nanoprecipitation¹¹ and hydrogel templated crystallization¹⁶ offer control over crystal domain size, powder flow properties and overall product uniformity. These product attributes make continuous pharmaceutical manufacture feasible, which in turn leads to decrease in production cost and waste generation and improvement in product quality and reliability.¹⁷

Hydrogels, water-swelling crosslinked polymer networks, as drug delivery vehicles offer solutions to several drug processing problems such as hydrophilicity,¹⁸ crystal size control,¹⁹ high drug loading²⁰ and predictable release.²¹ Moreover, the microporous environment of hydrogels can grant spatiotemporal control over chemical reactions and precipitation. One of the earliest examples of reaction-diffusion in the spatial confinement of a hydrogel is the Liesegang ring formation. In Liesegang's experiment, as a silver nitrate solution diffused through gelatin containing potassium chromate, distinct rings of silver chromate precipitate were formed.^{22,23} Biomineralization, a process through which bones are formed, also involves nucleation and crystallization of biominerals like calcium phosphate or calcium carbonate within hydrogel-like organic matrices.^{24,25} One of the strategies for co-processing salt APIs within polymeric composites is to use ion-exchange resins as carriers.^{11,26,27} Ion-exchange resins consist of a cross-linked polystyrene back bone with charged sites, which can be used to tether ionizable APIs to the polymer to obtain a taste-masking effect. The formulation outcome, however, is a drug-resinate complex that behaves differently from the original salt API in terms of release mechanism.²⁸ Another strategy for co-processing of salt APIs is to combine salt formation and amorphous solid

dispersions. The process involves performing the acid-base reaction in presence of a polymer excipient followed by solvent extraction.^{29,30} Reaction and precipitation in 3D confinement of a hydrogel matrix has not been widely explored in the context of API salt formation. This may be attributed to the fact that hydrogels are viewed as "aqueous" swelling polymeric meshes making them incompatible with processes occurring primarily in organic solvents. Interestingly, PEG-based hydrogels exhibit swelling in organic solvents^{31,32} due to the unique solubility profile of PEG and can therefore potentially serve as reservoirs for API salt formation.

In this contribution, a facile method to perform reactive crystallization of an API in presence of a spherical hydrogel template is developed. With the intent of improving the physical properties of the co-processed API, spherical hydrogel particles of $\sim 350 \mu\text{m}$ (microgels) served as templates. Cross-linked PEG diacrylamide (PEGDAAm) was chosen as the polymer owing to its hydrolytic stability.³³ The 3D hydrogel network porosity was enhanced by addition of an inert porogen, PEG (M_n 35,000), resulting in sufficient void space to allow for the reactants to be loaded and for precipitation to occur. Raltegravir-potassium was chosen as a model salt API for this study due to its straightforward reaction procedure, high reaction yield and poor physical properties. Raltegravir (N-(2-(4-(4-fluorobenzylcarbamoyl)-5-hydroxy-1-methyl-6-oxo-1,6-dihydropyrimidin-2-yl) propan-2-yl)-5-methyl-1,3,4-oxadiazole-2-carboxamide), an integrase inhibitor used for treatment of HIV infection, is a weak acid in its free phenol form (raltegravir-H). It is formulated as a crystalline potassium (K^+) salt owing to its superior exposure profile and aqueous solubility compared to the crystalline free form.³⁴ Raltegravir-H has a pK_a of 6.6 and can form a stable salt with strong bases like sodium hydroxide and potassium hydroxide.⁴ Industrially, the reaction is performed in bulk (Fig. 1a). Starting with a saturated solution of raltegravir-H in a suitable solvent, it is reacted with potassium hydroxide (KOH) dissolved in ethanol, methanol or water following which precipitation occurs spontaneously and the

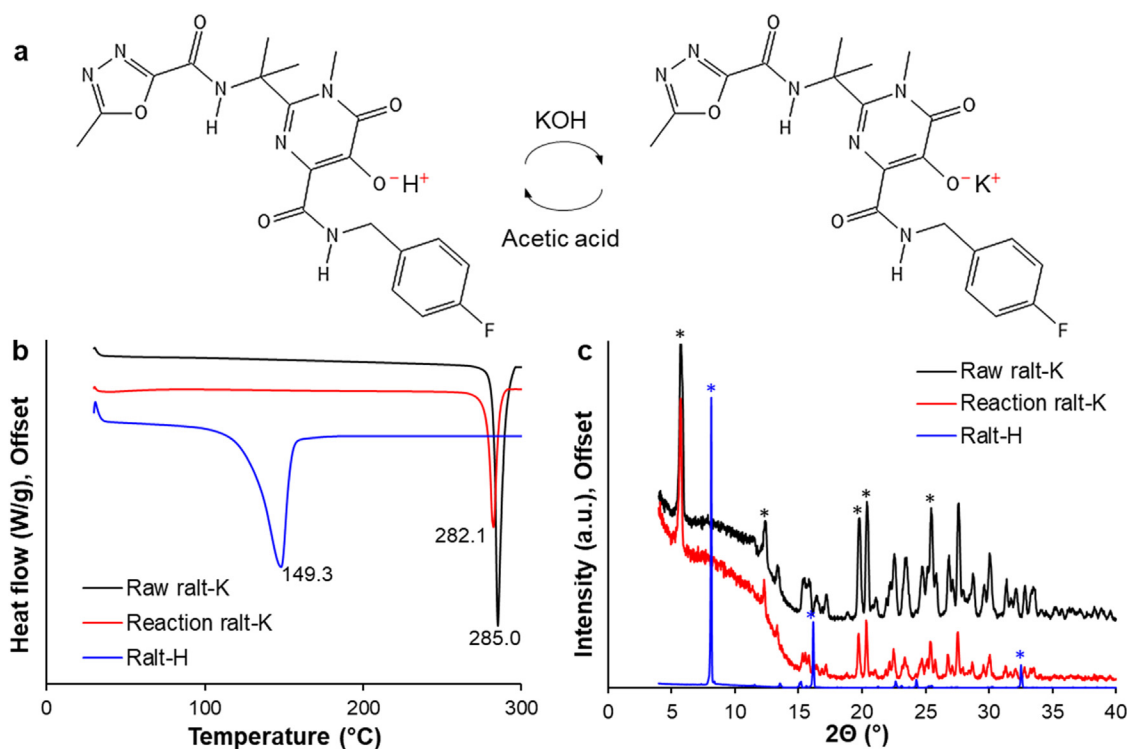


Figure 1. a. Reaction of raltegravir-H (ralt-H) with KOH to form raltegravir-K (ralt-K) and reverse reaction between ralt-K and acetic acid to form ralt-H, b. DSC thermograms showing melting profiles of ralt-H obtained from reaction between ralt-K and acetic acid, raw ralt-K and ralt-K obtained from reaction between ralt-H and KOH and c. PXRD spectra of ralt-H obtained from reaction between ralt-K and acetic acid, raw ralt-K and ralt-K obtained from reaction between ralt-H and KOH.

bulk salt crystals are dried.^{35,36} After isolation, the bulk crystalline raltegravir-K is micronized. This comes with challenges as there is some form conversion and chemical degradation sensitivity of the amorphous material generated during milling. While raltegravir-K boasts of improved aqueous solubility, it still has a non-ideal morphology which makes downstream processing difficult. As seen in Figure S1, raw raltegravir-K presents as a polydisperse powder with large high aspect ratio crystals and smaller low aspect ratio crystals. The micronized material is granulated using roller compaction to mitigate poor flow properties with additional surfactant to improve gastric solubility.³⁷ In this study, the reactants, raltegravir-H and KOH were added to dry hydrogel microparticles and allowed to react to form microgel-raltegravir-K composites. As the particles were washed with excess acetone to eliminate the reactants and dried, the microparticles exhibited de-swelling, causing raltegravir-K crystals to form a pleated precipitate along the hydrogel surface. The raltegravir-K microparticles have been characterized for morphology, drug distribution, crystallinity, release and flowability. Overall, our strategy offers a unique approach towards performing reactive crystallization within hydrogel micropores, leading to a free flowing material with promising dissolution performance, not needing downstream granulation and avoiding the spiral milling step which represents an additional unit operation, appreciable labor and overhead, yield loss, phase conversion and chemical stability challenges.

Experimental Section

Materials

Raltegravir-potassium (raltegravir-K) was obtained from Merck & Co., Inc., Rahway, NJ, 07,065, USA. Glacial acetic acid, acetone, potassium hydroxide (KOH), 2-propanol, ethanol, poly(ethylene glycol) diacrylamide (PEGDAAm) (Mn 3700), poly(ethylene glycol) (PEG) (Mn 35,000), Pluronic F127, silicone oil (10 cSt) and Irgacure 2959 were purchased from Sigma-Aldrich and were used without further purification. Ultrapure water (18.2 M Ω) was obtained using a Millipore Milli-Q purification system. Teflon tubing (1 mm I.D.) was purchased from GL Sciences and Teflon tee (1/16 inch orifice) was purchased from IDEX Corporation.

Synthesis of Raltegravir Free Form (Raltegravir-H)

A 0.124 M solution of raltegravir-K in ultrapure water was placed in a glass vial on a magnetic stirrer. Glacial acetic acid was added to the solution (1:1 v/v) and allowed to stir at 500 rpm till a visibly clear suspension was obtained. The glass vial was then refrigerated at 4 °C overnight to sediment raltegravir-H crystals. The crystals were washed subsequently with ultrapure water 5 times. The washed raltegravir crystals were dried overnight in a vacuum oven at 10 mbar pressure and $T = 80$ °C.

Synthesis of Raltegravir-K

Raltegravir-H in acetone (0.1 M) and KOH in 2-propanol (0.1 M) were added in 1:1 vol ratio in a glass vial vortexed for 5 s and left undisturbed. Visible turbidity was recorded at approximately 2 min and 30 s. After 30 min, the formed precipitate was isolated by centrifugation, washed with acetone and vacuum dried.

Microgel Fabrication

PEGDAAm microparticles were prepared by UV-crosslinking aqueous droplets containing the pre-polymer and photoinitiator generated by droplet microfluidics. A 20 mgmL⁻¹ stock solution of Irgacure 2959 was prepared in methanol and used as photoinitiator. The

aqueous dispersed phase comprised of 1% w/v Pluronic F127, 10% w/v PEGDAAm, 10% w/v PEG 35,000 and Irgacure 2959 (2 mgmL⁻¹) in ultrapure water. The continuous phase used was silicone oil (10 cSt). The continuous and dispersed phases were fed into the Teflon tee at flow rates of 200 μ Lmin⁻¹ and 20 μ Lmin⁻¹ respectively. The droplets were then subjected to a UV lamp (365 nm, 2 \times 15 W) at a distance of \sim 0.5 cm for 20 s. The spherical hydrogel microparticles were collected and washed with ethanol to remove any excess reactants and silicone oil.

Reaction in Presence of PEGDAAm Microgels

First, PEGDAAm microgels were washed three times in 2-propanol and were vacuum dried to ensure absence of any moisture within the hydrogel microenvironment. Raltegravir-H in acetone (0.1 M) and KOH in 2-propanol (0.1 M) were mixed in 1:1 volume ratio and instantly added to the dried microgels. The swollen microgels were left undisturbed for 30 min and then rinsed with an excess of acetone to wash off any excess reactants. The raltegravir-K microparticles were isolated and vacuum dried.

Raltegravir-K Microparticle Morphology

Particle and crystal morphology were characterized using a field emission scanning electron microscopy (FESEM, 7610, JEOL). Prior to FESEM observation at operating voltage 5 kV, dried samples were cut with a scalpel to expose their internal morphology and sputter coated with a platinum layer. The spatial distribution of raltegravir-K in the microparticle was characterized using energy dispersive X-Ray spectroscopy (EDX). The spatial maps corresponding to potassium and fluorine were captured at an operating voltage of 10 kV. Narrow X-ray photoelectron spectroscopy (XPS) scans for identification of fluorine, potassium and carbon in the powder surface were performed using Kratos AXIS Ultra^{DL}D at base pressure of 10⁻⁹ Torr, working pressure 5 \times 10⁻⁹ Torr with a 75 Watt X-ray source of Mono Al K α at a scattering angle of 90° and dwell time of 100–400 ms.

Raman Mapping of Microparticles

Raman spectra of neat PEGDAAm microgels, raw raltegravir-K, raltegravir-H and raltegravir-K composite microparticles were acquired using Renishaw inVia confocal Raman microscope. The spectra were captured at 50 \times magnification, 532 nm laser wavelength. Furthermore, confocal Raman mapping was carried out for 316 \times 316 μ m size, at 175 μ m depth from particle top with a 2 μ m per point resolution. The characteristic Raman maps were acquired for raltegravir-K at 1640 cm⁻¹ and for the PEGDAAm at 845 cm⁻¹.

Raltegravir-K Polymorph Characterization

The polymorphism of crystalline raltegravir-K within the hydrogel microparticles was characterized by powder X-ray diffraction (XRD) ranging from a 2θ angle of 4°– 40° at a scan rate of 2° min⁻¹. The PEGDAAm raltegravir-K microparticles were characterized using Differential Scanning Calorimetry (DSC) in DSC25 with Tzero pans from TA instruments. Each sample was equilibrated at 30 °C for 5 min before heating from 30 to 320 °C at a rate of 10 °C min⁻¹. The raltegravir-K polymorph and loading (w/w) was further characterized using Modulated DSC in DSC25 with Tzero pans from TA instruments. Each sample was equilibrated at 0 °C for 5 min before heating from 0 to 315 °C at a rate of 2 °C min⁻¹, with modulation period of 120 s and amplitude of 1 °C.

Raltegravir-K Loading

The raltegravir-K mass loading (w/w) was determined using Cary 60 UV–Visible spectrophotometer. Approximately 4 mg of the raltegravir-K microparticles were placed in phosphate-buffered saline (PBS) and allowed to dissolve for 2 h. The loading was determined by comparing the measured UV–visible spectrum maxima at 330 nm to a calibration curve obtained in the concentration range of 1 to 100 $\mu\text{g mL}^{-1}$ raltegravir-K dissolved in PBS Figure S12a.

Fourier Transform Infrared (FTIR) Spectroscopy

The FTIR spectra of PEGDAAm microgels, raw raltegravir-K and PEGDAAm raltegravir-K microparticles were collected in the attenuated total reflectance (ATR) mode using a Bruker Vertex 70 FTIR spectrometer. The spectrum of each sample was the average of triplicate runs of 30 scans and a resolution of 4 cm^{-1} .

Drug Release Assay

The raltegravir-K composite microparticles were suspended in 10 mL of PBS. The mass of particles suspended in PBS was calculated to ensure that the final raltegravir-K concentration after drug release would remain at 60 $\mu\text{g mL}^{-1}$, which is well below the saturation concentration (60 mg mL^{-1}). The particles were stirred using an orbital shaker at 200 rpm at 37 °C throughout the dissolution study. At specified time points, 500 μL samples were temporarily taken out to measure the amount of raltegravir-K released using a Cary 60 UV–vis spectrophotometer. The concentration of raltegravir-K released was quantified using the UV absorbance at 330 nm. To characterize release of raltegravir-K in simulated gastric fluid (SGF), the powders were suspended in 30 mL of SGF. The SGF was prepared by dissolving NaCl in deionized water (35 mM) and then adjusted to pH 1.2 with diluted HCl. The mass of particles suspended in SGF was calculated to ensure that the final raltegravir-K concentration after drug release would remain at $\sim 100 \mu\text{g mL}^{-1}$, which is below the saturation concentration (1.4 mg mL^{-1}). The particles were stirred using an orbital shaker at 200 rpm at 37 °C throughout the dissolution study. At specified time points, 500 μL samples were temporarily taken out to measure the amount of raltegravir-K released using a Cary 60 UV–vis spectrophotometer. A calibration curve was plotted for absorbance values obtained at 300 nm in the concentration range of 1 to 50 $\mu\text{g mL}^{-1}$ raltegravir-K in SGF as shown in the Figure S12b. The concentration of raltegravir-K released was quantified using the UV absorbance at 300 nm.

Angle of Repose Measurement

Approximately 100 mg of the raw raltegravir-K or PEGDAAm powder or composite microparticles was placed in a paper funnel and released onto a measuring plate and the angle of repose from the created powder cone was imaged and analyzed using image J.

Results and Discussion

Reaction in Presence of Microgels

First, the acidic raltegravir-H was synthesized in bulk from raw raltegravir-K salt as shown in Fig. 1a. Glacial acetic acid was added to an equal volume of a raltegravir-K solution in ultrapure water and refrigerated overnight. Raltegravir-H crystals were isolated after washing with DI water and vacuum drying them. The raltegravir-H crystals exhibited a single melting endotherm at 149.3 °C in the differential scanning calorimetry (DSC) thermogram (Fig. 1b), pointing to the formation of a single polymorph, form A3.³⁵ The crystals were

further characterized by powder X-ray diffraction (XRD) for the characteristic crystalline peaks at 8.1, 16.2 and 32.7° 2θ (Fig. 1c). Subsequently, raltegravir-K was synthesized in bulk by reacting equimolar solutions of the previously obtained raltegravir-H in acetone and KOH in 2-propanol. Owing to its insolubility in both solvents, raltegravir-K precipitated out and the crystals were washed with acetone and vacuum dried. As shown in Fig. 1b and 1c, the synthesized raltegravir-K (Reaction ralt-K) was of the same polymorphic form (form 1) as the raw raltegravir-K. Both the powders exhibited a similar PXRD profile and an identical melting endotherm at ~ 285 °C. The raw raltegravir-K and reaction raltegravir-K powders were further subjected to modulated DSC at a slower ramp rate of 2 °C/min. In Figure S2, the non-reversing heat flow curves for the two powders exhibited melting endotherms at ~ 268 °C confirming the presence of the same polymorphic form of raltegravir-K in both the powders. This outcome confirmed the choice of the solvent system for obtaining the original raltegravir-K polymorph. The starting raw raltegravir-K, reaction raltegravir-K and the synthesized raltegravir-H were visualized using field emission scanning electron microscopy (FESEM). The crystals exhibited a wide size distribution with non-uniform morphology for raw raltegravir-K and raltegravir-H, and a needle-like morphology for reaction raltegravir-K (Figure S1).

To investigate the reaction kinetics, dilute solutions of raltegravir-H and KOH were mixed and evaluated using UV-visible spectroscopy. 1.5 μM solutions of raltegravir-H in acetone and KOH in 2-propanol were prepared and added sequentially to a cuvette which was then subjected to absorbance measurements at 20 s intervals (Figure S3). The appearance of a shoulder (~ 345 nm) in the absorbance spectrum of raltegravir-H indicated formation of the salt raltegravir-K. This was confirmed by comparing the reaction spectrum to that of raw raltegravir-K dissolved in acetone-2-propanol solvent shown in Figure S3b. As seen in the Figure S3a, the salt formation proceeded nearly instantly, within seconds. The salt precipitation kinetics were characterized visually and through dynamic light scattering (DLS). In Figure S3c, images of vials containing the reactants raltegravir-H in acetone and KOH in 2-propanol (0.1 M each) after mixing over vortex for 5 s are presented. At the 3-minute time point, turbidity due to precipitation was captured. The turbidity continued to increase as seen in the vials at the 5 and 7-minute time points. Moreover, upon mixing of the reactants in a cuvette and running DLS, light scattering began at ~ 3 min timepoint and a measurement was obtained as shown in Figure S3d. The reaction, therefore, proceeded much faster than precipitation.

In this work, porous microgels served as templates for the reactive crystallization of raltegravir-K. The template microgels were fabricated through UV crosslinking of aqueous PEGDAAm (Mn 3400) droplets generated using droplet microfluidics in a T-junction. To improve the swelling rate of the microgels, a porogen, PEG (Mn 35,000) was introduced in the aqueous pre-polymer phase. Specifically, the aqueous stream composed of PEGDAAm, PEG, Pluronic F127 and photoinitiator served as a dispersed phase that was sheared and emulsified in a T-junction upon contact with an immiscible continuous phase of silicone oil. The resulting droplets were subjected to UV photopolymerization in the outlet tubing (Fig. 2a). The formed microgels were collected and washed in ethanol. As seen in optical micrographs (Fig. 2b), the PEGDAAm microgels were transparent in wet condition and opaque in dry condition, allowing for a visual distinction between the swollen and collapsed state. The neat microgels exhibited a smooth morphology on the surface and the cross-section as seen in the FESEM images in Fig. 2c. In this work, orthogonal to typical aqueous-system hydrogel applications, PEGDAAm hydrogel was applied for precipitation of a salt API from an organic solvent system. PEG's unique solubility in organic solvents and its fabrication in the form of $\sim 350 \mu\text{m}$ spherical microgels (Figure S4a) enabled uptake of the API-saturated solution and complete swelling before significant precipitation occurred (< 2 min). The microgel, therefore,

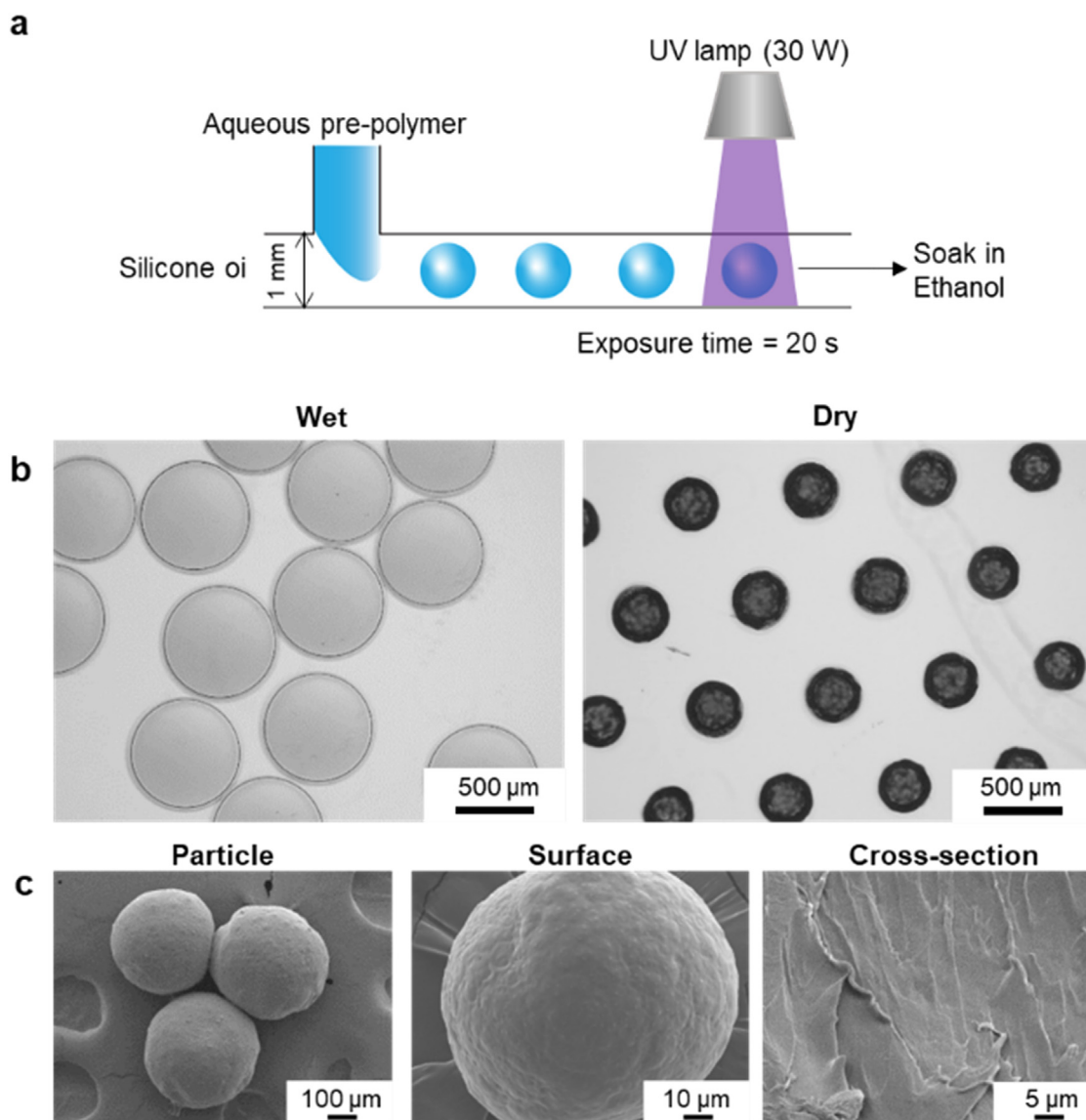


Figure 2. a. Schematic depicting the production of template PEGDAAm microgels through UV-crosslinking, b. Optical micrographs of swollen and dried PEGDAAm microgels, c. FESEM images of the neat PEGDAAm microgel surface and cross-section.

served as “mold” for the salt to precipitate in and did not necessarily induce crystallization.

For the reaction, the porous microgels were subjected to vacuum drying to extract all solvent and then re-swollen in the reaction solution containing equal parts of equimolar raltegravir-H in acetone and KOH in 2-propanol (Fig. 3a). The solution fed to the microgels was just enough to swell the dry microgels and any excess was extracted to avoid bulk precipitation on the microgel surface (Figure S5). As the microgels absorbed the reaction solution, precipitation of raltegravir-K proceeded in and around the microgel. After 30 min, the microgels were washed with excess of acetone, to wash away any unreacted species. The microgels exhibited de-swelling in excess acetone due to altered cross-link solubilization compared to the reaction solution followed by further de-swelling as they were dried. As a result, the microparticles exhibited a pucker surface with the raltegravir-K precipitate embedded in the hydrogel surface apparent from the FESEM images (Fig. 3b). The particle size distribution of the dry raltegravir-K-PEGDAAm microparticles indicated formation of spherical particles $\sim 310 \mu\text{m}$ in diameter (Figure S4b). The drastic particle de-swelling possibly caused the raltegravir-K crystals to aggregate at the

particle surface giving rise to a core-shell distribution of crystals in the raltegravir-K microparticles. This has been visualized through optical microscopy in video S1 and S2. The appearance of opacity in the transparent microgels upon acetone wash and drying was indicative of the formation of raltegravir-K.

Characterization of Raltegravir-K Microparticles

The presence of raltegravir-K on the surface of the microparticle and in the microparticle cross-section was confirmed by FESEM imaging, energy dispersive X-ray analysis (EDX), X-ray photoelectron spectroscopy (XPS) and confocal Raman mapping. As seen in Fig. 3b, precipitates were observed on the surface as well as embedded within the polymer matrix. The EDX maps (Fig. 4a) were generated for distribution of the elements potassium and fluorine on the surface and within the cross-section of the microparticle. The signal distribution indicated presence of the salt raltegravir-K on the surface as well as within the microparticle. High resolution XPS spectra were acquired to further characterize the presence of fluorine, potassium and carbon on the surface of raw raltegravir-K, raltegravir-H,

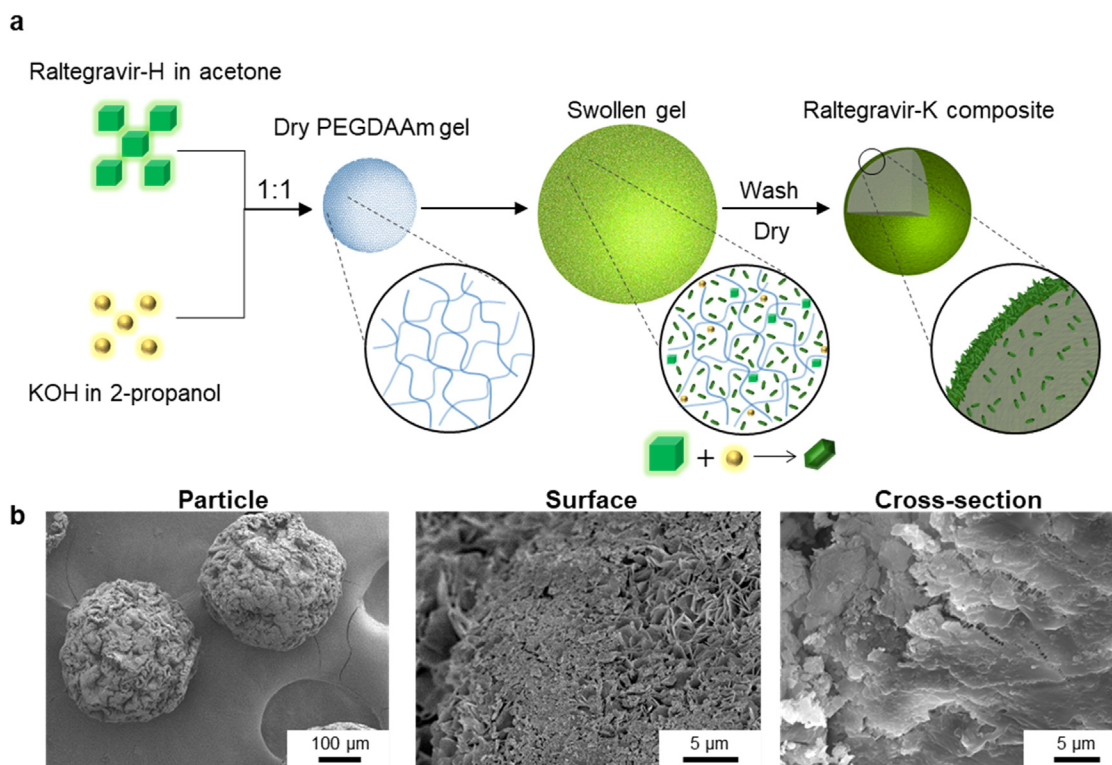


Figure 3. a. Schematic outlining the methodology of reacting ralte-H and KOH in the PEGDAAm hydrogel matrix, b. FESEM images of the PEGDAAm ralte-K microparticles. The left most image shows the overall particle morphology, the middle image shows the ralte-K crystals on the particle surface and the right most image shows precipitate in the particle cross-section.

PEGDAAm microgels and PEGDAAm raltegravir-K microparticles. As expected, fluorine signal F1s was found in raltegravir-H, raltegravir-K and PEGDAAm raltegravir-K microparticles (Figure S6a). Potassium signals corresponding to K1s and K2p were recorded in raw raltegravir-K and PEGDAAm raltegravir-K microparticles (Figure S6b, e, f). Carbon signal corresponding to electrons from C1s were found in all samples. This confirmed the presence of raltegravir-K on the surface of the PEGDAAm raltegravir-K microparticles.

For the confocal Raman mapping, individual Raman spectra of raw raltegravir-K and neat PEGDAAm microgels were acquired to identify characteristic Raman peaks for each (Figure S7). The confocal maps of the microparticles were generated at Raman shifts of 1640 cm^{-1} and 845 cm^{-1} corresponding to raltegravir-K and PEGDAAm respectively. While the Raman map of PEGDAAm showed a relatively uniform signal, the raltegravir-K map showed a higher crystal distribution on the microparticle surface compared to the cross-section (Fig. 4b). This was expected due to significant de-swelling exhibited by the microgel in the wash and dry step leading to preferential accumulation of the crystals on the surface.

A qualitative assessment for the presence of raltegravir-K within the microgel matrix was performed by addition of a dilute acetic acid solution to the raltegravir-K microparticles. The reaction between raltegravir-K and acetic acid yielded raltegravir-H within the particle cross-section, indicated by the appearance of opacity within the cross-section. When these microparticles were isolated and washed with acetone, the opacity disappeared confirming the formation of raltegravir-H (Figure S8). The composite microparticles were further visualized through polarized light microscopy in Figure S9. In contrast to the neat PEGDAAm microgels in Figure S9a, a diffuse layer of raltegravir-K crystals was observed on the surface of the dried microparticles in Figure S9b.

The crystallinity of raltegravir-K microparticles was characterized by XRD. Fig. 5a shows the powder XRD spectra of raw raltegravir-K,

raltegravir-H, neat PEGDAAm microgels and PEGDAAm raltegravir-K microparticles. The characteristic peaks of raw raltegravir-K and PEGDAAm were observed in the raltegravir-K microparticles as well. Specifically, peaks of 5.9 , 12.5 , 20.6 and $25.6^\circ 2\theta$ corresponding to raltegravir-K and peaks of 19.4 and $23.4^\circ 2\theta$ corresponding to PEGDAAm were recorded. The raltegravir-K microparticles were characterized by a DSC thermogram which exhibited two endotherms, one at 47°C corresponding to the melting of the crystalline PEG matrix and the other at 279.5°C corresponding to the melting of the raltegravir-K crystals (Fig. 5b). As seen in the DSC melting profile, both the melting endotherms of the composite PEGDAAm raltegravir-K particles exhibited a left shift of both PEG and raltegravir-K endotherms. This could be indicative of interaction between the drug and polymer. PEG is known to cause a melting point depression of various APIs when formulated as fused mixtures.^{38,39} However, no hydrogel based system has been explored for such drug-polymer interactions. As a preliminary characterization, the raw raltegravir-K, PEGDAAm microgels and PEGDAAm raltegravir-K microparticles were evaluated using IR spectroscopic analysis. As seen in the ATR-FTIR spectrum (Figure S10), the PEGDAAm raltegravir-K spectrum primarily exhibited the raltegravir-K peaks and lacked the characteristic PEGDAAm C—H stretching peak between 2800 and 2900 cm^{-1} and C—O stretching peak from 1000 to 1200 cm^{-1} . The absence of the polymer peaks could indicate an interaction between the raltegravir-K and PEGDAAm.

The raw raltegravir-K, reaction raltegravir-K and PEGDAAm raltegravir-K microparticles were further evaluated using modulated DSC (Figure S11) at a ramp rate of $2^\circ\text{C}/\text{min}$. The melting profile obtained through mDSC was then used for determining raltegravir-K loading of the microparticles. The loading of raltegravir-K in the microparticles was measured to be $34.1 \pm 4.4\%$ by mass of microparticles (Table S1). The loading of raltegravir-K in the microparticles was also analyzed through UV-visible spectroscopy and was found to be

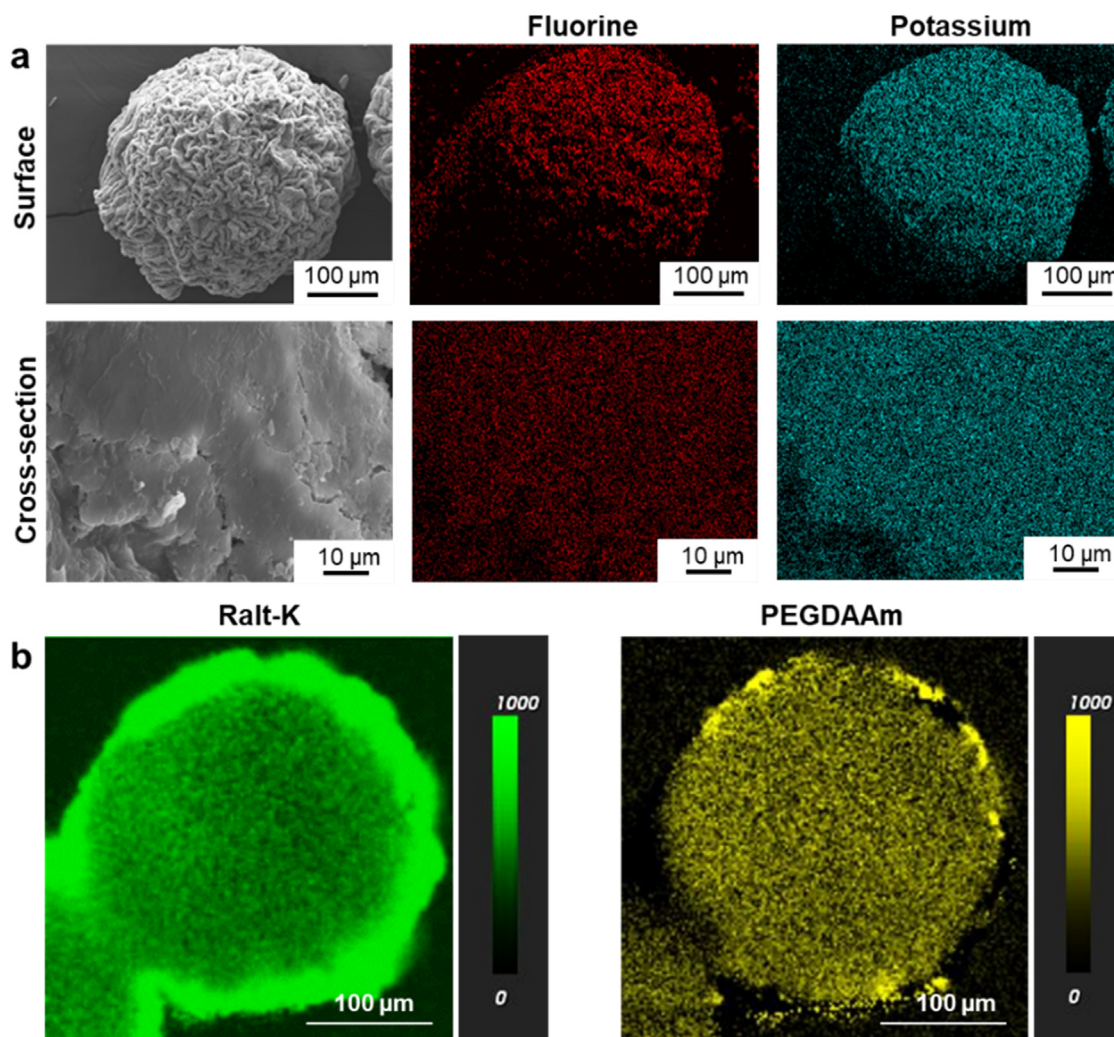


Figure 4. a. FESEM and EDX maps (fluorine and potassium) of the raltegravir-K crystals on the microparticle surface and in the particle cross-section, b. Confocal Raman maps for raltegravir-K (Ralt-K) at 1640 cm^{-1} and PEGDAAm at 845 cm^{-1} acquired at a distance $175\text{ }\mu\text{m}$ from the top of the particle.

$31.0 \pm 2.1\%$ by mass of microparticles. This indicated that the degree of crystallinity of raltegravir-K in the microparticles was $\sim 100\%$ (Section S11).

Drug Release

The release studies were carried out in phosphate-buffered saline (PBS) to simulate the oral cavity and in simulated gastric fluid (SGF) at pH 1.2. The microparticles were introduced into the PBS such that the final concentration of raltegravir-K in the solution would be approximately $60\text{ }\mu\text{g mL}^{-1}$, much lower than the saturation concentration at 60 mg mL^{-1} . This was done to maintain sink conditions throughout the study. Compared to the raw raltegravir-K dissolution profile, the release from the microparticles was slightly slower (Fig. 5c). This can be attributed to the outer crystalline shell dissolving immediately followed by dissolution of the crystals embedded within the hydrogel matrix. The raltegravir-K release from the PEGDAAm ralt-K microparticles was further characterized in SGF and compared to the dissolution profile of raw raltegravir-K. As seen in Fig. 5d, the release of raltegravir-K from the microparticles was slightly faster than raw raltegravir-K, contrary to the dissolution profile in PBS. Compared to PBS, raltegravir-K solubility in SGF is much lower.⁴⁰ Due to this, the dissolution of raltegravir-K was most likely affected by

its crystal domain size. The faster release from the microparticles could be attributed to the smaller crystal sizes in the composite microparticles compared to the raw raltegravir-K which is quite polydisperse (Figure S1). The time scale of release, however, was similar due to the high solubility of raltegravir-K in aqueous media and the hydrophilicity of the hydrogel matrix, promising bioavailability similar to the raw raltegravir-K formulation.

Angle of Repose

The flowability of a powder can be estimated by measuring its angle of repose. An angle of repose lower than 40° indicates good flowability and that greater than 40° indicates cohesiveness. The angles of repose of the raw raltegravir-K powder and the PEGDAAm raltegravir-K microparticles were determined by draining the powder through a funnel over a circular plate to form a gravimetric cone. As seen in Fig. 5e, the raw raltegravir-K powder exhibited a poor flowability with an average angle of repose of 51.2° . In contrast, the PEGDAAm raltegravir-K microparticles exhibited an improved flowability with an average angle of repose of 30.5° . This improvement indicates that the challenging physical properties of raltegravir-K can be addressed by co-processing it in the PEGDAAm hydrogel matrix to obtain spherical microparticles.

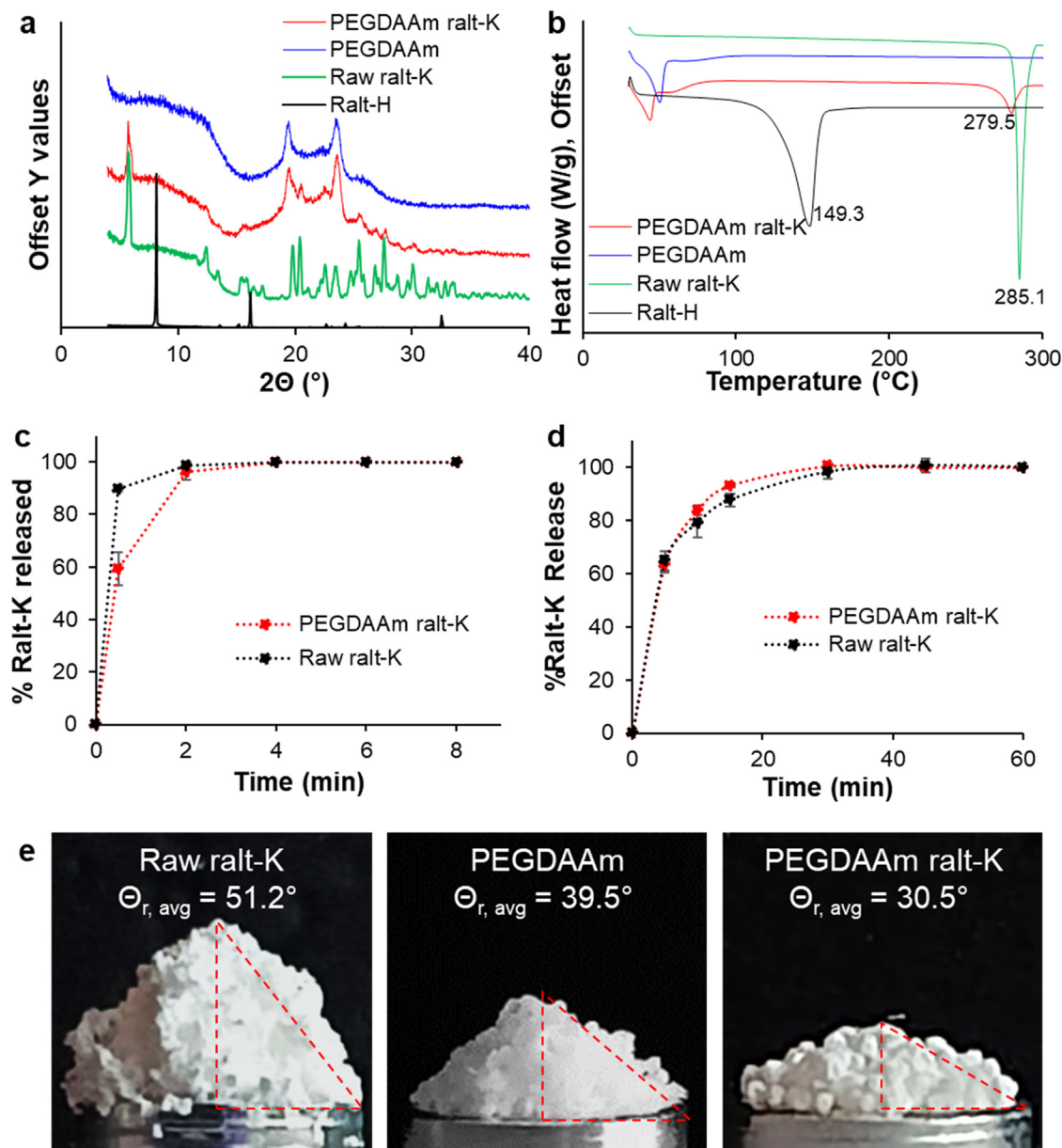


Figure 5. a. Powder XRD spectra of the neat PEGDAAm microgels, raw ralt-K, ralt-H and the PEGDAAm ralt-K microparticles, b. DSC thermogram of the neat PEGDAAm microgels, raw ralt-K, ralt-H and the PEGDAAm ralt-K microparticles, c. Ralt-K release from PEGDAAm ralt-K microparticles and raw ralt-K dissolution profile in PBS at 37 °C, d. Ralt-K release from PEGDAAm ralt-K microparticles and raw ralt-K dissolution profile in SGF at 37 °C, e. Average angle of repose ($\Theta_{r, avg}$) of raw ralt-K powder, PEGDAAm microgels and PEGDAAm ralt-K particles.

Conclusion

In this study, reactive crystallization of raltegravir-K was performed in presence of a non-ionic polymeric hydrogel matrix with the intent of improving manufacturability. While charged ionic resins or amorphous solid dispersions can serve as drug delivery strategies for ionizable APIs, they alter bioavailability of the original salt form significantly. Other porous carrier materials like silica particles, clay particles or alumina particles are insoluble in aqueous media, and when embedded with salt APIs can lead to poor bioavailability. Here a hydrolytically stable hydrogel of PEG diacrylamide served as porous template for precipitating salt raltegravir-K. The spherical microgels were swollen with organic solvent containing reacting acid-base precursors, allowing for highly localized precipitation in the matrix micropores. The resulting composite microparticles possessed

inherently micronized raltegravir-K precipitates on the surface as well as within the cross-section, which was a favorable outcome from the drug dissolution standpoint. These raltegravir-K precipitates were found to be crystalline and the microparticles exhibited improved flowability compared to the raw raltegravir-K powder. Due to hydrophilicity of the PEGDAAm hydrogel network, a burst release similar to the raw raltegravir-K form was obtained from the co-processed microparticles, promising an identical bioavailability.

Declaration of Competing Interest

The authors declare that they have no known competing financial interests or personal relationships that could have appeared to influence the work reported in this paper.

Acknowledgements

This research was supported by the Pharmaceutical Innovation Programme Singapore (grants number [A19B3a0012](#) and [M22B3a0051](#)).

Supplementary Materials

Supplementary material associated with this article can be found in the online version at [doi:10.1016/j.xphs.2023.05.004](https://doi.org/10.1016/j.xphs.2023.05.004).

References

- Merisko-Liversidge E, Liversidge GG. Nanosizing for oral and parenteral drug delivery: a perspective on formulating poorly-water soluble compounds using wet media milling technology. *Adv Drug Deliv Rev.* 2011;63(6):427–440. <https://doi.org/10.1016/j.addr.2010.12.007>.
- Müller RH, Keck CM. Twenty years of drug nanocrystals: where are we, and where do we go? *Eur J Pharm Biopharm.* 2012;80(1):1–3. <https://doi.org/10.1016/j.ejpb.2011.09.012>.
- Serajuddin ATM. Salt formation to improve drug solubility. *Adv Drug Deliv Rev.* 2007;59(7):603–616. <https://doi.org/10.1016/j.addr.2007.05.010>.
- Gupta D, Bhatia D, Dave V, Sutariya V, Varghese Gupta S. Salts of therapeutic agents: chemical, physicochemical, and biological considerations. *Molecules.* 2018;23(7):1719. <https://doi.org/10.3390/molecules23071719>.
- Altman R, Bosch B, Brune K, Patrignani P, Young C. Advances in NSAID development: evolution of diclofenac products using pharmaceutical technology. *Drugs.* 2015;75(8):859–877. <https://doi.org/10.1007/s40265-015-0392-z>.
- Paulekuhn GS, Dressman JB, Saal C. Trends in active pharmaceutical ingredient salt selection based on analysis of the orange book database. *J Med Chem.* 2007;50(26):6665–6672. <https://doi.org/10.1021/jm701032y>.
- McDonald MA, Salami H, Harris PR, et al. Reactive crystallization: a review. *React Chem Eng.* 2021;6(3):364–400. <https://doi.org/10.1039/D0RE00272K>.
- Schenck L, Koynov A, Cote A. Particle engineering at the drug substance, drug product interface: a comprehensive platform approach to enabling continuous drug substance to drug product processing with differentiated material properties. *Drug Dev Ind Pharm.* 2019;45(4):521–531. <https://doi.org/10.1080/03639045.2018.1562467>.
- Fatminia SMA, Wang Z, Liu B. Nanocrystallization: an effective approach to enhance the performance of organic molecules. *Small Methods.* 2017;1(3):1600023. <https://doi.org/10.1002/smdt.201600023>.
- Civati F, O'Malley C, Erxleben A, McArdle P. Factors controlling persistent needle crystal growth: the importance of dominant one-dimensional secondary bonding, stacked structures, and van der Waals contact. *Cryst Growth Des.* 2021;21(6):3449–3460. <https://doi.org/10.1021/acs.cgd.1c00217>.
- Schenck L, Erdemir D, Saunders Gorka L, et al. Recent advances in co-processed APIs and proposals for enabling commercialization of these transformative technologies. *Mol Pharm.* 2020;17(7):2232–2244. <https://doi.org/10.1021/acs.molpharmaceut.0c00198>.
- Paluch KJ, Tajber L, Adamczyk B, Corrigan OI, Healy AM. A novel approach to crystallisation of nanodispersible microparticles by spray drying for improved tabletability. *Int J Pharm.* 2012;436(1):873–876. <https://doi.org/10.1016/j.ijpharm.2012.05.074>.
- Ekdahl A, Mudie D, Malewski D, Amidon G, Goodwin A. Effect of spray-dried particle morphology on mechanical and flow properties of felodipine in PVP VA amorphous solid dispersions. *J Pharm Sci.* 2019;108(11):3657–3666. <https://doi.org/10.1016/j.xphs.2019.08.008>.
- Ng DZL, Nelson AZ, Ward K, Lai D, Doyle PS, Khan SA. Control of drug-excipient particle attributes with droplet microfluidic-based extractive solidification enables improved powder rheology. *Pharm Res.* 2022;39(2):411–421. <https://doi.org/10.1007/s11095-021-03155-0>.
- Nelson AZ, Kundukad B, Wong WK, Khan SA, Doyle PS. Embedded droplet printing in yield-stress fluids. *Proc Natl Acad Sci.* 2020;117(11):5671–5679. <https://doi.org/10.1073/pnas.1919363117>.
- Bora M, Hsu MN, Khan SA, Doyle PS. Hydrogel microparticle-templated anti-solvent crystallization of small-molecule drugs. *Adv Healthc Mater.* 2022;11(8):2102252. <https://doi.org/10.1002/adhm.202102252>.
- Fisher AC, Liu W, Schick A, et al. An audit of pharmaceutical continuous manufacturing regulatory submissions and outcomes in the US. *Int J Pharm.* 2022;622: 121778. <https://doi.org/10.1016/j.ijpharm.2022.121778>.
- Badruddoza AZM, Godfrin PD, Myerson AS, Trout BL, Doyle PS. Core-shell composite hydrogels for controlled nanocrystal formation and release of hydrophobic active pharmaceutical ingredients. *Adv Healthc Mater.* 2016;5(15):1960–1968. <https://doi.org/10.1002/adhm.201600266>.
- Chen L-H, Doyle PS. Design and use of a thermogelling methylcellulose nanoemulsion to formulate nanocrystalline oral dosage forms. *Adv Mater.* 2021;33(29):2008618. <https://doi.org/10.1002/adma.202008618>.
- Eral HB, López-Mejías V, O'Mahony M, Trout BL, Myerson AS, Doyle PS. Biocompatible alginate microgel particles as heteronucleants and encapsulating vehicles for hydrophilic and hydrophobic drugs. *Cryst Growth Des.* 2014;14(4):2073–2082. <https://doi.org/10.1021/cg500250e>.
- Chen L-H, Cheng L-C, Doyle PS. Nanoemulsion-loaded capsules for controlled delivery of lipophilic active ingredients. *Adv Sci.* 2020;7(20): 2001677. <https://doi.org/10.1002/advs.202001677>.
- Duley JM, Fowler AC, Moyles IR, O'Brien SGB. On the Keller–Rubinow model for Liesegang ring formation. *Proc R Soc A Math Phys Eng Sci.* 2017;473(2205): 20170128. <https://doi.org/10.1098/rspa.2017.0128>.
- Liesegang RE. *Naturwiss. Wochenschr.* 1896;11:353.
- Traub W, Arad T, Weiner S. Three-dimensional ordered distribution of crystals in turkey tendon collagen fibers. *Proc Natl Acad Sci U S A.* 1989;86(24):9822–9826. <https://doi.org/10.1073/pnas.86.24.9822>.
- Grassmann O, Müller G, Löbmann P. Organic–inorganic hybrid structure of calcite crystalline assemblies grown in a gelatin hydrogel matrix: relevance to biomineralization. *Chem Mater.* 2002;14(11):4530–4535. <https://doi.org/10.1021/cm0212156>.
- Borodkin S, Sundberg DP. Polycarboxylic acid ion-exchange resin adsorbates for taste coverage in chewable tablets. *J Pharm Sci.* 1971;60(10):1523–1527. <https://doi.org/10.1002/jps.2600601018>.
- Guo X, Chang R-K, Hussain MA. Ion-exchange resins as drug delivery carriers. *J Pharm Sci.* 2009;98(11):3886–3902. <https://doi.org/10.1002/jps.21706>.
- Jeong SH, Park K. Drug loading and release properties of ion-exchange resin complexes as a drug delivery matrix. *Int J Pharm.* 2008;361(1):26–32. <https://doi.org/10.1016/j.ijpharm.2008.05.006>.
- Van Duong T, HT Nguyen, Taylor LS. Combining enabling formulation strategies to generate supersaturated solutions of delamanid: in situ salt formation during amorphous solid dispersion fabrication for more robust release profiles. *Eur J Pharm Biopharm.* 2022;174:131–143. <https://doi.org/10.1016/j.ejpb.2022.04.002>.
- Haser A, Cao T, Lubach JW, Zhang F. In situ salt formation during melt extrusion for improved chemical stability and dissolution performance of a meloxicam–copovidone amorphous solid dispersion. *Mol Pharm.* 2018;15(3):1226–1237. <https://doi.org/10.1021/acs.molpharmaceut.7b01057>.
- Waters DJ, Engberg K, Parke-Houben R, et al. Morphology of photopolymerized end-linked poly(ethylene glycol) hydrogels by small-angle X-ray scattering. *Macromolecules.* 2010;43(16):6861–6870. <https://doi.org/10.1021/ma101070s>.
- Padmavathi NC, Chatterji PR. Structural characteristics and swelling behavior of poly(ethylene glycol) diacrylate hydrogels. *Macromolecules.* 1996;29(6):1976–1979. <https://doi.org/10.1021/ma950827r>.
- Stevens KR, Miller JS, Blakely BL, Chen CS, Bhatia SN. Degradable hydrogels derived from PEG-diacrylamide for hepatic tissue engineering. *J Biomed Mater Res A.* 2015;103(10):3331–3338. <https://doi.org/10.1002/jbm.a.35478>.
- Summa V, Petrocchi A, Bonelli F, et al. Discovery of raltegravir, a potent, selective orally bioavailable HIV-integrase inhibitor for the treatment of HIV-AIDS infection. *J Med Chem.* 2008;51(18):5843–5855. <https://doi.org/10.1021/jm800245z>.
- Kwokol A, Hedvati L, Burstein R, Yeori A, Moshkovits-Kapsan R. *Raltegravir Salts and Crystalline Forms Thereof*. Published online 2011. <https://patents.google.com/patent/WO2011123754A1/en?oq=WO+2011%2F123754+Al>.
- Belyk KM, Morrison HG, Jones P, et al. *Potassium Salt of an HIV Integrase Inhibitor*. 2006. Published Online; <https://patents.google.com/patent/US20060122205A1/en?oq=US+2006%2F0122205+A1>.
- Mahjour M, Smith RL. *Formulations of Raltegravir*. Published online 2021. <https://patents.google.com/patent/US20210290548A1/en?oq=US20210290548A1>.
- Law D, Wang W, Schmitt EA, Qiu Y, Krill SL, Fort JJ. Properties of rapidly dissolving eutectic mixtures of poly(ethylene glycol) and fenofibrate: the eutectic microstructure. *J Pharm Sci.* 2003;92(3):505–515. <https://doi.org/10.1002/jps.10324>.
- Baird JA, Taylor LS. Evaluation and modeling of the eutectic composition of various drug-polyethylene glycol solid dispersions. *Pharm Dev Technol.* 2011;16(3):201–211. <https://doi.org/10.3109/10837450903584936>.
- Moss DM, Siccardi M, Murphy M, et al. Divalent metals and pH alter raltegravir disposition in vitro. *Antimicrob Agents Chemother.* 2012;56(6):3020–3026. <https://doi.org/10.1128/AAC.06407-11>.